



Particle transport and heating in the microturbulent precursor of relativistic shocks

Illya Plotnikov, Guy Pelletier, Martin Lemoine

► To cite this version:

Illya Plotnikov, Guy Pelletier, Martin Lemoine. Particle transport and heating in the microturbulent precursor of relativistic shocks. Monthly Notices of the Royal Astronomical Society, 2013, 430, pp.1280-1293. <10.1093/mnras/sts696>. <insu-03617343>

HAL Id: insu-03617343

<https://insu.hal.science/insu-03617343v1>

Submitted on 25 Mar 2022

HAL is a multi-disciplinary open access archive for the deposit and dissemination of scientific research documents, whether they are published or not. The documents may come from teaching and research institutions in France or abroad, or from public or private research centers.

L'archive ouverte pluridisciplinaire **HAL**, est destinée au dépôt et à la diffusion de documents scientifiques de niveau recherche, publiés ou non, émanant des établissements d'enseignement et de recherche français ou étrangers, des laboratoires publics ou privés.



Distributed under a Creative Commons CC BY 4.0 - Attribution - International License

Particle transport and heating in the microturbulent precursor of relativistic shocks

Illya Plotnikov,¹★ Guy Pelletier¹★ and Martin Lemoine²

¹*UJF-Grenoble 1 / CNRS-INSU, Institut de Planétologie et d'Astrophysique de Grenoble (IPAG) UMR 5274, F-38041 Grenoble, France*

²*Institut d'Astrophysique de Paris, CNRS, UPMC, 98 bis boulevard Arago, F-75014 Paris, France*

Accepted 2012 December 21. Received 2012 October 23; in original form 2012 June 27

ABSTRACT

Collisionless relativistic shocks have been the focus of intense theoretical and numerical investigations in recent years. The acceleration of particles, the generation of electromagnetic microturbulence and the building-up of a shock front are three interrelated essential ingredients of a relativistic collisionless shock wave. In this paper, we investigate two issues of importance in this context: (1) the transport of suprathermal particles in the excited microturbulence upstream of the shock and its consequences regarding particle acceleration; (2) the preheating of incoming background electrons as they cross the shock precursor and experience relativistic oscillations in the microturbulent electric fields. We place emphasis on the importance of the motion of the electromagnetic disturbances relatively to the background plasma and to the shock front. This investigation is carried out for the two major instabilities involved in the precursor of relativistic shocks, the filamentation instability and the oblique two stream instability. Finally, we use our results to discuss the maximal acceleration at the external shock of a gamma-ray burst; we find in particular a maximal synchrotron photon energy of the order of a few GeV.

Key words: acceleration of particles – instabilities – relativistic processes – shock waves – gamma-ray burst: general.

1 INTRODUCTION

The microphysics of collisionless relativistic shocks has been intensively investigated in recent years, through both numerical simulations and theoretical investigations. As demonstrated in particular by Spitkovsky (2008a,b), the physics of these shock waves in the unmagnetized limit involves the interplay of three phenomena: the formation of the shock through the deceleration and reflection of particles against a microturbulent magnetic barrier, the self-generation of this microturbulence upstream of the shock by back scattered particles and the development of Fermi-type acceleration.

So far, particle acceleration has been observed in particle-in-cell (PIC) simulations of unmagnetized relativistic shocks (Spitkovsky 2008b; Keshet et al. 2009; Martins et al. 2009; Sironi & Spitkovsky 2009, 2011a), and indeed one must expect the development of the Fermi process when the magnetization is very weak, because microturbulence can then grow and provide the necessary scattering (Lemoine, Pelletier & Revenu 2006; Lemoine & Pelletier 2010). At larger levels of magnetization of the upstream flow, the shorter precursor scale may prevent the development of micro-instabilities, and in the absence of cross-field scattering, Fermi power laws cannot

develop (Lemoine, Pelletier & Revenu 2006; Niemec, Ostrowski & Pohl 2006); this picture has been validated in particular by the simulations of Sironi & Spitkovsky (2011a).

Nevertheless, the long time-scales and high energies that are inferred in powerful astrophysical sources remain well out of reach of these state of the art numerical simulations. It is therefore important to build on the basis of these numerical experiments a theoretical understanding of the various processes at play in these shock waves. In this work, we are interested in the physics of the microturbulence upstream of a relativistic weakly magnetized shock. Two fast growing micro-instabilities have received significant attention regarding the development of microturbulence upstream of a relativistic shock front: the filamentation (often termed Weibel) mode (e.g. Medvedev & Loeb 1999; Wiersma & Achterberg 2004; Lyubarsky & Eichler 2006; Achterberg & Wiersma 2007; Achterberg, Wiersma & Norman 2007; Bret 2009; Lemoine & Pelletier 2010, 2011a; Rabinak, Katz & Waxman 2011; Shaisultanov, Lyubarsky & Eichler 2012) and the two stream instability (hereafter OTSI; e.g. Bret, Firpo & Deutsch 2005; Bret 2009; Lemoine & Pelletier 2010, 2011a; Shaisultanov et al. 2012). Both instabilities follow from the interpenetration of the beam of back scattered particles and the incoming background plasma in the shock precursor (as viewed from the shock frame). One should nevertheless mention the possibility of a Buneman instability, if the returning particles carry a net current, which turns out to grow faster than the previous two, see

★ E-mail: illya.plotnikov@obs.ujf-grenoble.fr (IP); Guy.Pelletier@obs.ujf-grenoble.fr (GP)

e.g. Bret (2009) and Lemoine & Pelletier (2011a) for a discussion. However, the Buneman instability saturates through the heating of the background electrons, so that it presumably serves as an efficient source of preheating. In this work, we are mostly interested in the properties of particle transport (and energization) in the microturbulence upstream of a relativistic shock front and we will focus our discussion on the respective roles of the filamentation and two stream modes.

In the downstream, the microturbulence appears isotropic, mostly magnetic and static, see e.g. Chang, Spitkovsky & Arons (2008). The physics of transport of suprathermal particles in such a microturbulence, possibly superimposed on a weak background magnetic field, has been discussed in a previous paper (Plotnikov, Pelletier & Lemoine 2011). Upstream of the shock, this microturbulence is strongly elongated in the direction of the shock normal and in the background plasma rest frame, it carries both electric and magnetic fields. That must affect the transport properties of suprathermal particles in a non-trivial way and likely contribute to the heating of background electrons. Furthermore, we demonstrate in this work that the filamentation modes have a finite phase velocity in the background plasma rest frame, an issue which to our knowledge has not been addressed before in the present context. We find that this motion has important consequences regarding both the transport of suprathermal particles, in particular the acceleration time-scale, and the preheating of the background electrons, which turns out to be fast and efficient.

This paper is organized as follows. In Section 2, we discuss the motion of the frame in which the Weibel filaments are static, and we summarize previous findings on a similar issue for the OTSI mode. We investigate the influence of the motion of the electromagnetic modes on the reflection process at the shock front. In Section 3, we study the transport of suprathermal particles in both Weibel and OTSI turbulence, on the basis of numerical simulations of test particle propagation. We place emphasis on the issue of scattering in three dimensions. Section 4 discusses electron heating. We show that the relativistic oscillation of the incoming background electrons in the electric field of the microturbulence modes lead to efficient preheating on a short time-scale. In Section 5, we apply our results to the concrete case of the external relativistic shock of a gamma-ray burst (GRB). We summarize our results in Section 6.

2 MICROTURBULENCE IN THE PRECURSOR OF COLLISIONLESS WEAKLY MAGNETIZED RELATIVISTIC SHOCKS

We start with some definitions of key quantities. We note $\mu \equiv m_e/m_p$ the electron to proton mass ratio, Γ_s the Lorentz factor of the shock, n the density of the background (upstream) plasma, $\rho = nm_p c^2$ the rest-mass density, B_0 the magnetic field of the background plasma; θ_B the angle between the direction of \mathbf{B}_0 and the shock normal; these quantities are defined in the upstream plasma rest frame. The magnetization parameter is then defined as

$$\sigma \equiv \frac{B_{\parallel}^2}{4\pi\Gamma_s^2 \rho c^2} = \frac{B_0^2}{4\pi\rho c^2} \sin^2 \theta_B, \quad (1)$$

with $B_{\parallel} = \Gamma_s B_0 \sin \theta_B$ the transverse component of the background magnetic field in the shock front rest frame. Numerical simulations provide two essential parameters for astrophysical applications, namely the conversion factor ξ_{cr} of the incoming energy into

cosmic rays (suprathermal particles), and the conversion factor ξ_B into magnetic energy:

$$P_{cr} \equiv \xi_{cr} \Gamma_s^2 \rho c^2, \quad \frac{\bar{B}_{\parallel}^2}{4\pi} = \xi_B \Gamma_s^2 \rho c^2, \quad (2)$$

where the cosmic ray pressure P_{cr} and the level of magnetic turbulence \bar{B}_{\parallel} are measured at the shock front. These two crucial parameters ξ_{cr} and ξ_B are expected to be on the order of 1–10 per cent (Sironi & Spitkovsky 2011a). Actually the cosmic rays are considered, as shown by numerical simulations and explained by theory, as the source of magnetic, and more generally electromagnetic, turbulence. In the present context of a proton–electron plasma of low magnetization, the reference time-scale is ω_{pi}^{-1} and the spatial scale of reference is the inertial scale of protons $\delta_i \equiv c/\omega_{pi}$.

In this section, we present the essential characteristics of the filamentation instability and the oblique two stream instability, which are the most important sources of turbulence in the precursor of ultrarelativistic shocks. As briefly mentioned above, there are also Buneman instabilities that are triggered by the compensation current in the background plasma, which compensates the current carried by the reflected particles either along the mean field (for a parallel shock) or across the mean field. For instance, reflected particles of opposite charge rotate in the opposite direction in the transverse mean field and thus produce a very intense diamagnetic current responsible for a Buneman instability (Lemoine & Pelletier 2011a), which grows rapidly. Those current instabilities produce a turbulent heating of the electrons up to some temperature that reduces the anisotropy of the electron distribution function, up to the point where the instability saturates. Therefore, these current instabilities participate in the process of preheating electrons, which then arrive at the shock front with a relativistic temperature. In this paper, we will not address the preheating effect due to Buneman instability and focus on the Weibel and OTSI instabilities. In the picture that we develop here, these instabilities indeed push the preheating to higher temperatures, up to near equipartition, by the time the electrons reach the shock front.

The first generation of reflected particles constitutes the main content of suprathermal particles that penetrate the ambient plasma with an energy density much larger than ρc^2 as measured in the frame of the ambient plasma. Its interaction with the background plasma can be described perturbatively as long as the proton beam of (apparent) density n_b and Lorentz factor γ_b is such that $\omega_{pb} \ll \omega_p$, which amounts to $n_b/\gamma_b \ll n/\mu$. Now for a beam reflected by a shock, $n_b = \xi_{cr} \Gamma_s^2 n$ and $\gamma_b \sim \Gamma_s^2$; thus the weak interaction criterium becomes $\xi_{cr} \ll 1/\mu$, which is always realized. The weak interaction of the very energetic beam with the ambient (or upstream) plasma renders the calculation of the instability convenient in the frame of the background plasma.

2.1 The frame of magnetic filaments

Consider first the growth of magnetic perturbations due to the Weibel instability triggered by a parallel beam of velocity v_b and Lorentz factor $\gamma_b = (1 - v_b^2/c^2)^{-1/2} \sim \Gamma_s^2$ (upstream frame), interacting with a cold background plasma of density n at rest; at a shock wave, the beam of returning particles carries an energy density $\xi_{cr} \gamma_b^2 n m_p c^2$, so that the beam plasma frequency $\omega_{pb} \sim \xi_{cr}^{1/2} \mu^{1/2} \omega_{pe}$, with ω_{pe} the background electron plasma frequency (see Lemoine & Pelletier 2010 for details). In the upstream rest frame, the e-folding length-scale of the instability is written as

$$\ell_g \equiv c/\Im\omega \sim \xi_{cr}^{-1/2} \delta_i, \quad (3)$$

the detailed growth rate (see Appendix A) being

$$\gamma_{\text{inst}} \equiv \Im \omega = \sqrt{\xi_{\text{cr}} \omega_{\text{pi}}} \frac{\beta_b k_{\perp} \delta_e}{(1 + k_{\perp}^2 \delta_e^2)^{1/2}}. \quad (4)$$

In the above expression and throughout this paper, k_{\perp} represents the wavenumber component transverse to the shock normal, i.e. tangential to the shock front, while the (longitudinal) wavenumber component along the shock normal is written k_{\parallel} . For the filamentation mode, $k_{\perp} \gg k_{\parallel}$. In general, one takes the limit $k_{\parallel} \rightarrow 0$, which leads to an aperiodic mode, i.e. $\Re \omega = 0$. However, for a small, but finite longitudinal wavenumber k_{\parallel} , the Weibel modes have a non-vanishing real frequency which indicates that these magnetic filaments propagate at high velocity. Considering first the above case of a cold electron background,

$$\omega_r \equiv \Re \omega = k_{\parallel} v_b \left(1 - \xi_{\text{cr}} \mu \frac{\gamma_b^{-2} + k_{\perp}^2 \delta_e^2}{1 + k_{\perp}^2 \delta_e^2} \right). \quad (5)$$

We remark that this phase velocity is consistent with the result obtained in the centre of mass frame of the counter streaming configuration when $\gamma_b \simeq 1$; for $\mu = 1$ and $\xi_{\text{cr}} = 1/2$, we find a phase velocity $v_b/2$ at peak growth rate, which corresponds to a vanishing phase velocity in the centre of mass frame.

In this work, we will often refer to the wave frame, which corresponds to the frame moving at the phase velocity of the magnetic disturbance $v_m \equiv \beta_m c$ along the shock normal direction:

$$\beta_m \equiv \frac{\Re \omega}{k_{\parallel} c}. \quad (6)$$

By definition, the wave is static in this frame, since the mode frequency in that frame $\omega' = \gamma_m (\omega - k_{\parallel} v_m) = 0$, with $\gamma_m = (1 - \beta_m^2)^{-1/2}$. Strictly speaking, this phase velocity is not unique because of its dependence on k_{\perp} ; however, we consider it for the most unstable mode, which introduces only a small dispersion $\Delta \beta_m / \beta_m \sim \xi_{\text{cr}} \mu$.

In the above cold background plasma limit, the Weibel filaments can be considered as wave packets of transverse size $\ell_{\perp} \sim \delta_e$ and extension in the normal direction $\ell_{\parallel} > \delta_e$, but necessarily finite (at least because of the finite growth length in a precursor of finite extent). Equation (5) indicates that these filaments move at a high speed relatively to the ambient medium. Indeed,

$$\gamma_m \simeq (\xi_{\text{cr}} \mu)^{-1/2} \sim 140, \quad (7)$$

where the numerical value holds for an electron–proton plasma with $\xi_{\text{cr}} = 0.1$. This is an important point, which has not been taken into account in the literature, to our knowledge. The motion of the wave packets indeed carries particular importance when determining the condition for particle reflection, the level of electron preheating and also for the analysis of the Fermi process, as discussed in the following.

In the upstream rest frame, these waves are quasi-electromagnetic waves with the electric field \mathbf{E} mostly oriented along the beam (shock normal), a dominant magnetic component perpendicular to both \mathbf{k}_{\perp} and \mathbf{E} , and finally a small electrostatic component of \mathbf{E} along \mathbf{k}_{\perp} . The magnetic component remains the most intense component despite a phase velocity close to c along the normal direction because $E/B \simeq (\xi_{\text{cr}} + k_{\parallel}^2 \delta_i^2)^{1/2} / (k \delta_i)$. The fact that they have a phase velocity close to c implies that they suffer negligible Landau damping, at least as long as the thermal velocity of the electrons is small.

The filaments are static in the frame moving at β_m with respect to the background plasma; however, in their rest frame they are no

longer predominantly magnetic. They actually possess an electrostatic field of almost the same intensity as the magnetic field, as a standard Lorentz transform shows: $E'_{\perp} \simeq \gamma_m B \simeq B'$, since $B' = \gamma_m B$, with the prime denoting the quantity in the filament rest frame. This electrostatic field turns out to be an important source of heating for the background electrons, as discussed in Section 4.

If the background electrons have been preheated to relativistic temperatures, their electromagnetic response and therefore the instability are modified. The maximum growth rate remains unchanged, $\Im \omega \sim \xi_{\text{cr}}^{1/2} \omega_{\text{pi}}$, but the spatial scale at which maximum growth occurs is now larger because the electron inertial scale is enlarged by a factor $\sqrt{\bar{\gamma}_e}$, with $\bar{\gamma}_e$ the mean electron thermal Lorentz factor in the upstream rest frame $\bar{\gamma}_e = 1 + 3T_e/m_e c^2$. Detailed calculations are given in Appendix A; they include in particular Landau damping on hot electrons, which essentially reduces the growth rate at larger wavelengths. This latter spatial scale tends to δ_i in the limit of equipartition, meaning $\bar{\gamma}_e \rightarrow m_p/m_e$. In a relativistically hot background, the phase velocity of the modes along the beam direction is slowed down, but nonetheless remains relativistic for reasonable values. The calculations presented in Appendix A indicate

$$\gamma_m \simeq [(\bar{\gamma}_e \mu \xi_{\text{cr}})^{1/2} + 2\xi_{\text{cr}}]^{-1/2}. \quad (8)$$

Equipartition corresponds to $\bar{\gamma}_e \mu = 1$; therefore, prior to equipartition $\bar{\gamma}_e \mu < 1$. For relativistically hot electrons far from equipartition, $\gamma_m \simeq (2\xi_{\text{cr}})^{-1/2}$, then $\gamma_m \sim (\xi_{\text{cr}} \mu \bar{\gamma}_e)^{-1/4}$ when $\bar{\gamma}_e \mu > \xi_{\text{cr}}$, and finally the lowest value of $\gamma_m \sim 2$ is reached at equipartition. This value is significantly smaller than that obtained in the cold electron background, $\gamma_m \sim (\xi_{\text{cr}} \mu)^{-1/2}$, but it nevertheless plays an important role in what follows.

Note that the filamentation instability in the upstream of a relativistic shock is quenched when $\Gamma_s < (\xi_{\text{cr}} \mu)^{-1/2}$ as long as the electrons are kept cold due to the finite angular dispersion of the beam (Lemoine & Pelletier 2011a; Rabinak et al. 2011). In a hot background, however, the filamentation instability remains strong, even when the beam angular dispersion is taken into account.

The above discussion shows that the velocity of the filaments depends on the degree of preheating of the background electrons, hence on the distance to the shock front, since electrons are cold at the tip of the precursor and hot at the shock transition, see Sironi & Spitkovsky (2011a). Three cases deserve attention: $\gamma_m \sim \Gamma_s$ where the filaments move more or less at the same speed as the shock front, $\gamma_m < \Gamma_s$ where the shock front catches up the filaments and the case where the filaments can even run faster than the shock for $\Gamma_s < \gamma_m$. In this latter case, the generation of filaments might lead to shock reformation, but this issue is not discussed here.

The relative velocity of the filaments with respect of the shock front can be written as

$$\beta_{\text{m|f}} \simeq \frac{\gamma_m^2 - \Gamma_s^2}{\gamma_m^2 + \Gamma_s^2}, \quad (9)$$

and the associated Lorentz factor

$$\Gamma_{\text{m|f}} \simeq \frac{1}{2} \left(\frac{\gamma_m}{\Gamma_s} + \frac{\Gamma_s}{\gamma_m} \right). \quad (10)$$

The discussion about the motion of magnetic disturbances is also important for their transmission to the downstream flow. Indeed, the relative motion of the upstream flow with respect to the downstream one is characterized by a relative Lorentz factor $\Gamma_r = \Gamma_s / \sqrt{2}$. The Lorentz transform of the frequency and normal wavenumber of

filaments to the downstream frame leads to

$$\begin{aligned}\omega_{\parallel d} &= \Gamma_r(\beta_m - \beta_r)k_{\parallel}c \simeq \frac{1}{2}\Gamma_r k_{\parallel}c \left(\frac{1}{\Gamma_r^2} - \frac{1}{\gamma_m^2} \right) \\ k_{\parallel d} &= \Gamma_r(1 - \beta_r\beta_m)k_{\parallel} \simeq \frac{1}{2}\Gamma_r k_{\parallel} \left(\frac{1}{\Gamma_r^2} + \frac{1}{\gamma_m^2} \right).\end{aligned}\quad (11)$$

Thus, when $\gamma_m \ll \Gamma_s$, the modes are perceived as electromagnetic vacuum waves in the downstream frame, propagating backwards ($\omega_{\parallel d} \simeq -k_{\parallel d}c$). However, one should stress here that the motion of the filament is calculated at the linear level, while the transmission of modes downstream proceeds in the highly non-linear regime. Therefore, it is not clear at present whether the above equation 11 applies to the transition; it should be taken with caution.

Finally, in the case of an ultrarelativistic shock in an electron positron plasma, γ_m is at most a few and the shock front catches up the magnetic disturbances ($\Gamma_s \gg \gamma_m$). The behaviour is the same in a proton–electron plasma at near equipartition.

2.2 The role of OTSI turbulence

Although the Weibel instability can produce all the effects expected to occur at a relativistic shock, the OTSI appears unavoidable, and it grows a little bit faster than the Weibel instability at least in the cold background limit. The OTSI is a resonant instability of electron plasma waves ($\omega \simeq \omega_{pe}$) with a sharp selection of the wavevector component along the beam: $k_{\parallel} = \omega_{pe}/c$, which grows much faster than the usual two stream instability when the transverse component of the wavevector is also of the order of ω_{pe}/c (e.g. Fainberg, Shapiro & Shevchenko 1970; Bret et al. 2005). These modes are mostly electrostatic in the background plasma frame; their frequency is slightly shifted off resonance according to: $\Re\omega = \omega_{pe}(1 - |\delta|/2)$ and their growth rate $\Im\omega = \sqrt{3}2^{-4/3}|\delta|\omega_{pe}$ with $|\delta| = \xi_{cr}^{1/3}\mu^{1/3}$ (e.g. Lemoine & Pelletier 2010, 2011a). The ratio of the electromagnetic component over the electrostatic one is of the order of $|\delta|$.

As discussed in Lemoine & Pelletier (2011a) and Shaisultanov et al. (2012), the two stream instability becomes inhibited once the electrons are heated to ultrarelativistic temperatures and the Weibel instability becomes the dominant mode.

In order to study the dynamics of particles in the modes, it is interesting to move to the wave frame in which the particles experience a static electric field and a static magnetic field. The wave frame velocity with respect to the background plasma $\beta_m = 1 - |\delta|/2$ and the corresponding Lorentz factor:

$$\gamma_m \simeq |\delta|^{-1/2} \simeq \xi_{cr}^{-1/6} \mu^{-1/6} \sim 5, \quad (12)$$

with respect of the background plasma. These mildly relativistic wave packets are thus rapidly overtaken by the shock front.

As in the case of Weibel modes, the dynamics in OTSI modes is also governed by a couple of transverse fields of similar amplitude when one shifts to the rest frame in which these modes are static. A crucial difference however is that the OTSI mode appears as a high-frequency quasi-vacuum monochromatic wave in the front frame, revealing a clear periodic pattern in the direction of the shock normal.

2.3 Suprathermal particles, the background plasma and the shock

In Sections 3 and 4 that follow, we address, respectively, the issues of the scattering of suprathermal particles and the heating process of background particles in the motional microturbulence upstream of

the shock. These actually represent two different facets of a similar problem, namely particle transport in a time varying microturbulence. However, in the test particle picture that we adopt in the following, these two populations, the suprathermal particles and the background electrons, differ one from the other by their wiggler parameter:

$$a \equiv \frac{e\bar{E}'\ell'_{\perp}}{m_e c^2}, \quad (13)$$

as expressed in terms of the microturbulent electric field \bar{E}' and transverse scale ℓ'_{\perp} in the wave frame. As discussed in the following, in the wave frame \bar{E}' and \bar{B}' are of the same order, so that there is no ambiguity in the definition of a .

Cold background electrons have a Lorentz factor $\gamma' \sim \gamma_m$ in the wave frame, so that

$$\frac{a}{\gamma'} \simeq \xi_B^{1/2} \frac{m_p}{m_e} \frac{\ell_{\perp}}{\delta_i} \gg 1, \quad (14)$$

meaning that these electrons experience relativistic oscillations on a coherence length-scale in the wave frame. Of course, as the electrons near equipartition, the ratio a/γ' becomes closer to unity.

In sharp contrast, the same wiggler parameter for suprathermal particles $a/\gamma' \ll 1$. To see this, consider a suprathermal electron, with Lorentz factor γ in the upstream rest frame, becoming $\gamma' \simeq \gamma/\gamma_m$ in the mode rest frame (assuming $\gamma \gg \gamma_m$). The minimal Lorentz factor of suprathermal electrons is $\gamma_{\min} \sim \Gamma_s^2 m_p/m_e$ in the upstream frame, hence one can write

$$\frac{a}{\gamma'} \simeq \xi_B^{1/2} \frac{\gamma_m^2}{\Gamma_s^2} \frac{\gamma_{\min}}{\gamma} \frac{\ell_{\perp}}{\delta_i}, \quad (15)$$

which is indeed expected to be much smaller than unity: recall that ℓ_{\perp} is expected of the order of δ_e if the background electrons are cold (in which case γ_m can be large if the Weibel instability is not quenched by the angular dispersion of the beam), but of the order of δ_i if the background electrons reach equipartition with the ions, in which case γ_m becomes of the order of a few for the Weibel modes. Thus, $a/\gamma' \ll 1$ for suprathermal electrons, while $a/\gamma' \gg 1$ for the background electrons, typically.

For similar reasons, the microturbulence cannot trap the suprathermal protons and thereby saturate the ion filamentation instability that these particles seed. This would require that the level of microturbulence is such that the time-scale of non-linear oscillation τ_{nl} in the filament becomes comparable to the growth time-scale $\Im\omega \sim \omega_{pb}^{-1}$. This oscillation time-scale can be expressed as $\tau_{nl} = \ell'_{\perp}(\gamma'/a)^{1/2}/c$ and $\omega_{pb} = \xi_{cr}^{1/2}\omega_{pi}$, so that one would need $a/\gamma' \simeq \xi_{cr}^{-1}(\ell_{\perp}/\delta_i)^2$ for suprathermal particles, which cannot be satisfied. A similar conclusion can be drawn when one considers the resonance broadening effect, which stems from the fact that particle scattering or diffusion broadens the resonance of modes with the beam responsible for the instability.

Presumably, the Weibel instability in the shock precursor does not actually saturate, but it stops growing once the incoming (background) plasma ions are turned around by the microturbulent field, as viewed in the shock front rest frame. At this point, the shock transition actually takes place. This notably implies that the back scattered particles are roughly isotropic at this location (again, as viewed in the shock front frame). This and the near isotropy of the incoming ions, as they are turned around, then imply the end of growth of the Weibel instability. Interestingly, this argument leads to a level of magnetic turbulence which agrees well with current simulations.

This can be seen as follows, in the upstream rest frame in which the filamentation modes are mostly static. In a first approximation, the transverse magnetic field can be described as coherent in the shock normal direction on a growth length-scale $c/\Im\omega$. An incoming proton is turned around on this length-scale provided

$$\frac{e\bar{B}}{m_p c} \approx \Im\omega, \quad (16)$$

and $\Im\omega = \omega_{pb}$ for the filamentation instability implies a level

$$\frac{\bar{B}^2}{4\pi} \approx \xi_{cr} n m_p c^2, \quad (17)$$

meaning $\xi_B \approx \xi_{cr}$ at the shock front. The above agrees rather satisfactorily with the PIC simulations of Sironi & Spitkovsky (2011a). Of course, the actual time to reach this amplitude, starting from some background fluctuation value far upstream, is of the order of $\Im\omega$ times an e-folding factor of the order of a few to 10.

3 TRANSPORT OF SUPRATHERMAL PARTICLES IN THE WAVE FRAME

The properties of particle transport in microturbulence has been already studied downstream of a relativistic shock (e.g. Chang et al. 2008; Plotnikov et al. 2011). There, the transport coefficients are found to depend essentially on a scattering frequency, which scales as the square of the particle energy, corresponding to small pitch-angle scattering:

$$v_{sld} = \frac{2}{3} \frac{c}{\ell_{cld}} \left(\frac{e\bar{B}_{ld}}{\epsilon_d} \right)^2, \quad (18)$$

with ℓ_{cld} the coherence scale, \bar{B}_{ld} the total magnetic field and ϵ_d the particle energy, in the downstream frame. In the absence of a mean field, spatial diffusion is isotropic and is simply described by the standard diffusion coefficient:

$$D \simeq c \ell_{cld} \left(\frac{\epsilon_{ld}}{e\bar{B}_{ld} \ell_{cld}} \right)^2. \quad (19)$$

However, spatial diffusion is anisotropic in the presence of a mean field; then, the transverse diffusion coefficient tends towards a constant value as the particle energy becomes large (Plotnikov et al. 2011).

Upstream, the situation is rather different, notably because of the anisotropy of the microturbulence.

In the upstream frame, the wavenumbers of Weibel modes obey $k_{\perp}/k_{\parallel} \gg 1$ and $\Re\omega \ll k_{\perp}$, so that $k'_{\perp}/k'_{\parallel} \gg 1$ in the wave frame as well. Regarding OTSI modes, one finds $k_{\perp} \sim k_{\parallel}$ in the upstream frame, but Lorentz boosting to the wave frame gives predominance to the transverse wavenumbers. If, in a first approximation, the spatial dependence along the shock normal is disregarded, the normal component of the generalized momentum becomes a constant of motion in the wave frame: $p_{\parallel} + eA_{\parallel}(x, y) = C$ (where C is a constant, A_{\parallel} the parallel component of the electromagnetic vector potential). In this frame, the total energy is also a constant of motion due to time translation invariance. Thus, the momentum of the particle is confined in a subset of the energy surface determined by $\Delta p_{\parallel} = e\Delta A_{\parallel}$, where ΔA_{\parallel} is the rms variation of the normal vector potential (wave frame). In short, the assumption of translational invariance along the Weibel filaments leads to an inhibition of momentum diffusion, see also Jones, Jokipii & Baring (1998) for similar issues. This is a crucial point which directly impacts the efficiency of acceleration, which requires transverse scattering in the absence of a mean field. As we discuss further below, the

transverse momentum is subject to large angular variations in the transverse plane, which leads to spatial diffusion. In order to obtain pitch angle diffusion, it is thus necessary to consider the full 3D dependence of the magnetic fluctuations.

For both Weibel and OTSI modes, the analysis of particle dynamics is more suitable in the wave frame, because this is the frame in which the transport coefficients can be properly defined, where the distribution function tends to become more or less isotropized, and fundamentally, this is the proper frame of scattering centres involved in the Fermi process. Henceforth, all quantities are therefore evaluated in the frame of magnetic disturbances, unless otherwise stated.

The electromagnetic components in the wave frame are derived from those calculated upstream at the linear level by the Lorentz transforms:

$$\begin{aligned} E'_{\parallel} &= E_{\parallel} \\ E'_{\perp} &= \gamma_m (E_{\perp} + \beta_m \times B_{\perp}) \\ B'_{\parallel} &= B_{\parallel} \\ B'_{\perp} &= \gamma_m (B_{\perp} - \beta_m \times E_{\perp}). \end{aligned} \quad (20)$$

In the case of Weibel modes, $|E| \ll |B|$, and for γ_m large enough, $B'_{\perp} \simeq \gamma_m B_{\perp}$ and $E'_{\perp} \simeq \gamma_m \beta_m \times B_{\perp} \simeq \beta_m \times B'_{\perp}$.

In the case of OTSI modes, in the upstream frame the modes are almost electrostatic $|B| \ll |E|$, and $E_{\perp} \sim E_{\parallel}$ (oblique modes). The system is quite similar to the system derived for Weibel modes in their proper frame, since $E'_{\perp} \simeq \gamma_m E_{\perp}$ and $B'_{\perp} \simeq -\gamma_m \beta_m \times E_{\perp}$, which leads to $B'_{\perp} \simeq -\beta_m \times E'_{\perp}$.

Below, we analyse the particle dynamics first in a 2D approximation, meaning $E'_{\parallel} \rightarrow 0$, $B'_{\parallel} \rightarrow 0$, and then in the complete 3D configuration ($E'_{\parallel} = E'_{\perp}/\gamma_m$). When going to the wave frame, the perpendicular coherence length remains unchanged, $\ell'_{\perp} = \ell_{\perp}$, while $\ell'_{\parallel} = \gamma_m \ell_{\parallel}$.

3.1 Transport in 2D approximation

Defining as z the direction of the shock normal, the system can be written as:

$$\frac{dp_x}{dt} = q E'_x (1 + \beta_m \beta_z) \quad (21)$$

$$\frac{dp_y}{dt} = q E'_y (1 + \beta_m \beta_z) \quad (22)$$

$$\frac{dp_z}{dt} = -q \beta_m (\beta_x E'_x + \beta_y E'_y) \quad (23)$$

where the relation $B'_{\perp} = -\beta_m \times E'_{\perp}$ has been inserted, and the fields E'_{\parallel} and B'_{\parallel} have been discarded in a first approximation. Because $\omega' = 0$ or $\omega = k_z v_m$, $k'_z = \gamma_m (k_z - \beta_m \omega/c) = k_z/\gamma_m$, and thus for large γ_m the z dependence of the field can be neglected in a first approximation. The system is the same for both Weibel and OTSI modes.

As discussed above, there are two invariants: the total particle energy $H = \epsilon(p) + q\Phi(x, y)$ written in terms of a Hamilton function with electromagnetic potential Φ , and the generalized momentum component along z , $\pi_z = p_{\parallel} + qA_z(x, y)/c$. These two potentials are related to one another: $A_z(x, y) = \Phi(x, y)$. Since the potential has a zero average and a finite rms value $\Delta\Phi$, the particle proper energy ϵ and its z -momentum p_{\parallel} have well-defined rms variations under the ergodic assumption: $\Delta\epsilon = \Delta p_{\parallel} c = e\Delta\Phi$. These relations

determine confinement regions in phase space and forbid some diffusion processes. The norm of the transverse momentum also has bounded variations. Indeed, considering the variation from initial values, $\delta\epsilon = \epsilon - \epsilon_0$, $\delta p_{\parallel} = p_{\parallel} - p_{\parallel,0}$, $\delta p_{\perp} = p_{\perp} - p_{\perp,0}$, one exactly finds

$$2(\epsilon_0 - p_{\parallel,0}c)\delta\epsilon = c^2(\delta p_{\perp})^2. \quad (24)$$

Now because $p_{\perp,0}$ is small, this constraint allows large variations of the polar angle of p_{\perp} . Thus, the variations of the energy and momenta are bounded, except for the angle of the transverse momentum that can vary randomly over the interval $(0, 2\pi)$; those erratic variations of the angle can occur with the β_z contribution to the transverse equations of motions that opens phase space with another degree of freedom.

It proves convenient to define the reference energy:

$$\epsilon_{\star} \equiv e\tilde{E}'\ell_{\perp} \equiv am_e c^2. \quad (25)$$

As discussed before, $a/\gamma' \ll 1$ for suprathermal particles, meaning that $\epsilon_{\star} \ll \epsilon$. Such particles are strongly beamed forward along the shock normal in the upstream frame; in the wave frame, $p_{\perp,0}/p_{\parallel,0} \lesssim \gamma_{\text{mif}}/\Gamma_s$ implies $p_{\perp,0} \ll p_{\parallel,0}$ for typical values of γ_{mif} , hence $\epsilon_0 \simeq p_{\parallel,0}c$ initially. The transport of suprathermal particles can then be described as the random walk of a *non-relativistic* particle in the transverse plane, coupled to ballistic motion along the longitudinal direction. In the transverse plane, the particle is described as non-relativistic because its transverse velocity $v_{\perp} \simeq p_{\perp}/p_{\parallel} \ll 1$ and, given that $\epsilon_{\star} \ll p_{\parallel,0}c$, the particle cannot exchange a large fraction of its parallel momentum with transverse momentum due to the invariance properties in this 2D approximation.

The transverse motion, devoid of linear resonance but governed by a continuum of Fourier modes, is thus characterized by a single non-linear time:

$$t_{\text{nl}} \equiv \frac{\ell_{\perp}}{c} \left(\frac{2p_{\parallel,0}c}{\epsilon_{\star}} \right)^{1/2}. \quad (26)$$

This is the time needed to cross a coherence cell for a particle that gets accelerated transversely in the transverse electric field. Over a coherence length, the electric field can be considered as constant and the particle receives a transverse kick $c\Delta p_{\perp} \sim \epsilon_{\star}$.

If the initial transverse momentum $p_{\perp,0} \ll \epsilon_{\star}/c$, the spatial transverse motion can be approximated by

$$\Delta x_{\perp} \simeq \frac{1}{2} \frac{eE_{\perp}}{p_{\parallel,0}} ct^2 + v_{\perp,0}t, \quad (27)$$

since the kick remains much smaller than $(\epsilon_{\star}p_{\parallel,0})^{1/2}$; $v_{\perp,0} \equiv p_{\perp,0}/p_{\parallel,0}$. The non-linear time so defined is the time beyond which the non-linear dynamics de-correlates the trajectories. It can also be considered as the time-step for a random deflection of angle θ_i in the transverse plane since each crossing of a coherence cell in the transverse direction is associated with a large variation of θ_i when $p_{\perp,0} \ll \epsilon_{\star}/c$. Thus, after n steps of size ℓ_{\perp} , the trajectory has diffused such that

$$\langle \Delta x_{\perp}^2 \rangle \simeq \frac{1}{2} \ell_{\perp}^2 n, \quad (28)$$

with $n \simeq \Delta t/t_{\text{nl}}$, which leads to a transverse spatial diffusion coefficient:

$$D_{\perp} \simeq \frac{1}{4} \frac{\ell_{\perp}^2}{t_{\text{nl}}} \propto p_{\parallel,0}^{-1/2}. \quad (29)$$

If $p_{\perp,0}c \gg \epsilon_{\star}$, the transverse velocity undergoes small variation of its modulus in the crossing of a coherence cell, but it can undergo

significant angle variations. This transverse quasi-scattering can be analysed in two regimes: (a) when $p_{\perp,0}c \ll (\epsilon_{\star}p_{\parallel,0})^{1/2}$ and (b) when $p_{\perp,0}c \gg (\epsilon_{\star}p_{\parallel,0})^{1/2}$ but still $p_{\perp,0} \ll p_{\parallel,0}$. In the former limit, the particle crosses a transverse coherence cell in a non-linear time-scale as previously, whereas in the latter case the crossing occurs on a linear time-scale $\ell_{\perp}/|v_{\perp}|$. Let us estimate the transverse diffusion coefficient for both cases. In case (a), when crossing a coherence cell, the particle undergoes a small transverse deflection of angle $\theta_i \sim \epsilon_{\star}/p_{\perp}c$. The scattering time is therefore longer than t_{nl} with $t_{\text{scatt}} \sim \theta_i^{-2}t_{\text{nl}}$ and diffusion in the transverse plane during $\Delta t > t_{\text{scatt}}$ is such that

$$\langle \Delta x_{\perp}^2 \rangle \sim \frac{\ell_{\perp}^2}{2} \left(\frac{t_{\text{scatt}}}{t_{\text{nl}}} \right)^2 \frac{\Delta t}{t_{\text{scatt}}}. \quad (30)$$

This indicates that, in this regime of small deflection, a particle travels over a much larger distance than ℓ_{\perp} during a scattering time, namely $(t_{\text{scatt}}/t_{\text{nl}})\ell_{\perp}$. The transverse diffusion coefficient is thus

$$D_{\perp} \sim \frac{1}{4} \frac{\ell_{\perp}^2}{t_{\text{nl}}} \left(\frac{p_{\perp}c}{\epsilon_{\star}} \right)^2. \quad (31)$$

In case (b), the small deflection that occurs during the linear correlation time leads to a scattering time $t_{\text{scatt}} \sim \theta_i^{-2}\ell_{\perp}/v_{\perp}$. And the transverse diffusion coefficient becomes:

$$D_{\perp} \sim \frac{1}{4} v_{\perp} \ell_{\perp} \left(\frac{p_{\perp}c}{\epsilon_{\star}} \right)^2. \quad (32)$$

3.2 Numerical results in 2D approximation

The system of equations of motions in the fields is solved by the Bulirsch–Stoer algorithm (Press et al. 1986), together with statistics over a sample of random phases and polarization directions of plane waves. The field \mathbf{E}'_{\perp} is decomposed in plane waves with the constraint $\mathbf{k}' \parallel \mathbf{E}'_{\perp}$, which implies that \mathbf{k}' is in the plane (x, y) , choosing as before the normal direction along the z -direction. In this subsection, we set $k'_z = 0$ and $E'_z = 0$ in the wave frame. Several hundreds of modes are used. The system converges quite rapidly with $\sim 10^3$ particles. For simplicity, we investigate only the case where the initial particle momentum is oriented along the parallel direction, $\mathbf{p}_0 = p_{\parallel,0}\mathbf{e}_z$.

All simulations use the following units: the spatial length unit is $m_e c^2/(eE'_{\text{rms}})$ (E'_{rms} is the rms of the electric field strength), the time unit is $m_e c/(eE'_{\text{rms}})$ and momenta are expressed in units of $m_e c$. The coherence length $\ell_{\perp} = 1$ in these units, so that $\epsilon_{\star} = m_e c^2$.

Numerical results are presented in Figs 1 and 2. Fig. 1 depicts the time evolution of spatial diffusion coefficients for different $p_{\parallel,0}/(m_e c)$ in a 2D approximate geometry. Green curves depict the time evolution in the parallel direction and blue curves represent the same quantity in the transverse direction. Displacements in the parallel direction are clearly ballistic: $\langle \Delta x_{\parallel}^2 \rangle = v_{\parallel,0}^2 t^2$. In the transverse plane, at least two regimes are identified: for $t < t_{\text{nl}}$, $\langle \Delta x_{\perp}^2 \rangle \propto t^4$ as expected from particle acceleration by nearly constant electric field over its coherence cell, see equation (27); for $t > t_{\text{nl}}$, $\langle \Delta x_{\perp}^2 \rangle/\Delta t$ reaches a plateau (i.e. diffusion) and its value has a power-law dependence on $p_{\parallel,0}$ with a slope of $-1/2$ (see the sub-panel of the figure), which fits well the result of the previous section, see equation (29). This behaviour is a direct consequence of particle trapping in every coherence cell it encounters, with a ‘waiting time’ per cell being equal to t_{nl} . The case where $p_{\perp,0}$ is different from zero was also investigated. In this case, there is no more trapping in the field coherence cell but random motions in the transverse plane.

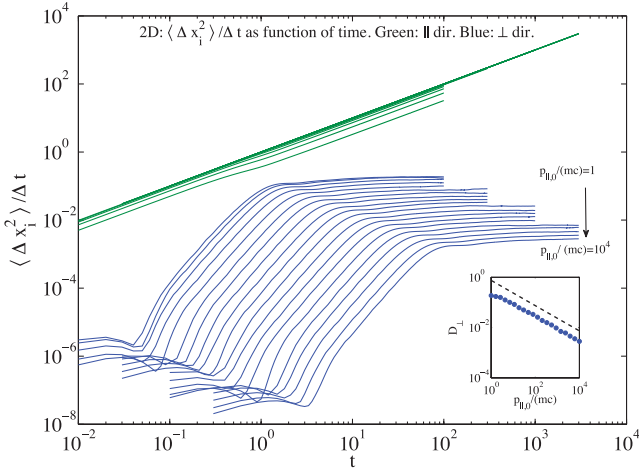


Figure 1. Time evolution of spatial diffusion coefficients for different $p_{\parallel,0}/(mc)$ in 2D fields geometry approximation. Green curves: parallel direction; blue curves: transverse direction $[(x, y) \text{ plane}]$. Displacements in the parallel direction are clearly ballistic: $\langle \Delta x_{\parallel}^2 \rangle = v_{\parallel,0}^2 t^2$. In the transverse plane, at least two regimes are identified: when $t < t_{nl}$, $\langle \Delta x_{\perp}^2 \rangle \propto t^4$ as expected from particle acceleration by nearly constant electric field over its coherence cell; when $t > t_{nl}$, $\langle \Delta x_{\perp}^2 \rangle / \Delta t$ reaches a plateau (i.e. diffusion) and its value has a power-law dependence on $p_{\parallel,0}$ with a slope of $-1/2$ (see subpanel). Subpanel: transverse diffusion coefficient (plateau) dependence on initial particle momentum $p_{\parallel,0}$. The dashed line follows the power-law slope $-1/2$.

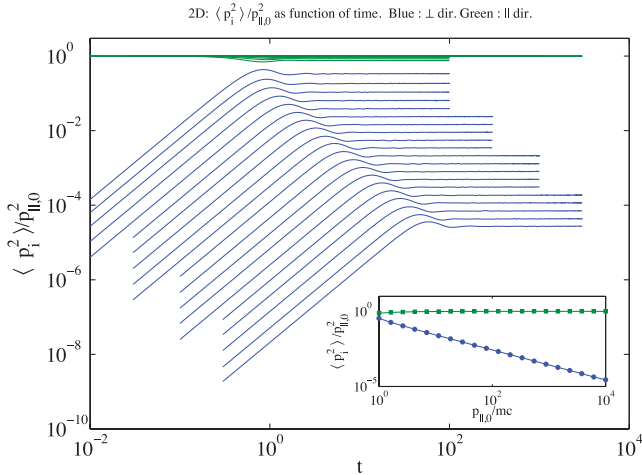


Figure 2. Time evolution of $\langle p_i^2 \rangle / p_{\parallel,0}^2$ for different values of $p_{\parallel,0}/(mc)$, in 2D approximation. Green curves: parallel (z) direction; blue curves: transverse direction. Subpanel: asymptotic values of $\langle p_i^2 \rangle / p_{\parallel,0}^2$ as function of $p_{\parallel,0}$. $\langle p_{\parallel}^2 \rangle / p_{\parallel,0}^2$ is slightly inferior to 1 independently from $p_{\parallel,0}$ (green squares). In transverse direction (blue circles) $\langle p_{\perp}^2 \rangle / p_{\parallel,0}^2 \propto p_{\parallel,0}^{-1}$.

We obtain a diffusive behaviour on longer time-scales as discussed in the previous section (e.g. equations 30, 31).

Fig. 2 presents the evolution of $\langle p_{\parallel}^2 \rangle / p_{\parallel,0}^2$ (green curves) and $\langle p_{\perp}^2 \rangle / p_{\parallel,0}^2$ (blue curves) as function of time for different $p_{\parallel,0}/(mc) \in [1, 10^4]$. There is no diffusion in momentum space with parallel component being bounded by the π_z invariant, while the transverse one varies as $\langle \Delta p_{\perp}^2 \rangle / (mc)^2 \propto p_{\parallel,0}$. Since the generalized momentum is constrained by this π_z invariant, we expect a transverse momentum gain $\langle \delta p_{\perp}^2 \rangle = e E'_{\perp} \ell_{\perp} p_{\parallel,0} / c$.

Finally, we can mention that the energy gain $\langle \Delta \gamma \rangle$ is independent of $p_{\parallel,0}$ and corresponds to the amount of energy brought by the rms electric field potential. It can be expressed as $\langle \Delta \gamma \rangle = e E'_{\perp} \ell_{\perp}$. The energy variation from $\epsilon(p_{\parallel,0})$ to $\epsilon(p_{\parallel,0}) + q E'_{\perp} \ell_{\perp}$ takes place when $0 < t < t_{nl}$. For $t > t_{nl}$, the particle energy remains constant.

3.3 Transport in 3D fields

We consider now the particle transport over a longer time-scale, for the full 3D geometry, i.e. including a single resonant mode with $k_z = \delta_e^{-1}$ in the case of OTSI and a continuum of small wave numbers in the case of Weibel modes. In the wave frame, the longitudinal coherence length $\ell'_{\parallel} \simeq \gamma_m \ell_{\parallel}$, and $\ell_{\parallel} \sim \ell_{\perp}$ for OTSI modes in the background plasma frame, so that $\ell'_{\parallel} \simeq \gamma_m \ell'_{\perp}$. For Weibel modes, $\ell_{\parallel} \sim \delta_i / \xi_{cr}^{1/2}$ and $\ell_{\perp} \sim \xi_B^{1/2} \delta_i$, thus $\ell_{\parallel} / \ell_{\perp} \sim \xi_{cr}^{-1}$ and therefore $\ell'_{\parallel} / \ell'_{\perp} \sim \gamma_m / \xi_{cr} \gg 1$.

The invariance of the generalized z -momentum is now broken and the particle momentum can diffuse in all directions. One limitation is the phase-space confinement due to the total energy conservation that forbids energy diffusion. Another is that the longitudinal coherence length is significantly larger than the coherence length in the transverse direction. With respect to the above 2D analysis, we thus expect a change of regime when the spatial variation in the z -direction is felt by the particle, which corresponds to time-scales much larger than ℓ'_{\parallel} / c . The randomization of the longitudinal component of the momentum is then expected over a time t_z , with

$$t_z \simeq \frac{\ell'_{\parallel}}{c} \left(\frac{p_{\parallel,0} c}{e E'_{\perp} \ell'_{\parallel}} \right)^2 \simeq \frac{\ell'_{\parallel}}{\ell'_{\perp}} \frac{\ell'_{\perp}}{c} \left(\frac{p_{\parallel,0} c}{\epsilon_{\star}} \right)^2. \quad (33)$$

For both OTSI and Weibel modes, $E'_{\perp} \ell'_{\parallel} \simeq E'_{\perp} \ell'_{\perp}$ because in the wave frame, $\nabla \times \mathbf{E}' = 0$. The above is a linear estimate of the scattering time-scale in the longitudinal direction; however, simulations at low energies suggest that the dependence on ℓ'_{\parallel} differs from this latter. We will take into account that the lack of knowledge by introducing a factor χ measuring the delay, compared to the 2D correlation time, of the full development of 3D dynamics. It turns out to impact directly the maximal acceleration energy.

Over intermediate time-scales, we expect to recover the previous results about the transverse diffusion and no diffusion in the longitudinal direction. But on time-scale longer than t_z , one expects a 3D diffusion with

$$D_{\perp} = \frac{1}{3} \ell'_{\perp} c \left(\frac{p_{\parallel} c}{\epsilon_{\star}} \right)^2, \quad D_{\parallel} = \frac{\ell'_{\parallel}}{\ell'_{\perp}} D_{\perp}. \quad (34)$$

As before, we assumed that the deflection over a coherence cell is small with $\delta \theta \sim \epsilon_{\star} / p_{\parallel,0} c$. The description of the expected behaviours of these diffusion regimes is provided in the figures shown in the next paragraph.

3.4 Numerical results in 3D fields

We take the same configuration as in the 2D case but with a finite value of $E'_{\parallel} = E'_{\perp} / \gamma_m$ in the case of OTSI, with $k'_{\parallel} / k'_{\perp} = 1 / \gamma_m$. To simulate a Weibel turbulence, we include an ensemble of modes, consistent with the original wave equations of Weibel modes,

$$E'_{\parallel}(k'_{\parallel}) = -\frac{k'_{\parallel}}{k_{\perp}^2} (\mathbf{k}'_{\perp} \times \mathbf{B}'_{\perp}) \cdot \boldsymbol{\beta}_m, \quad (35)$$

which insures the conservation of the total energy of each particle. For this ensemble of Weibel modes, $k'_{\parallel} / k'_{\perp}$ takes small values up to

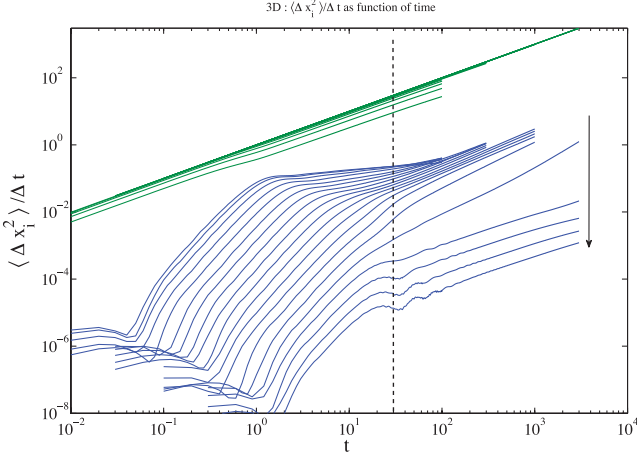


Figure 3. Transverse spatial diffusion in 3D modes of OTSI type. This graph depicts the time evolution of spatial diffusion coefficients for different $p_{\parallel,0}/(m_e c)$ in 3D fields. Green curves: parallel (z) direction; blue curves: transverse direction [(x, y) plane]. The dashed vertical line delimits the linear coherence time in z-direction $t_{\parallel,c} = \gamma_m l_{\perp} / c$. Displacements in the parallel direction remain ballistic on numerical time-scales, since the integration time is too short to probe the diffusive behaviour in this direction. In the transverse direction, 2D-like diffusive behaviour (see Fig. 1) disappears gradually when $t_{\text{nl}} < t < t_z$.

some parameter $\kappa < 1$; consequently, $E'_{\parallel}/E'_{\perp} \sim \kappa$. Most numerical calculations were done with the same time-scales as in the 2D case.

Fig. 3 depicts the time evolution of spatial diffusion coefficients for different $p_{\parallel,0}/(m_e c)$ in 3D OTSI fields, assuming $\gamma_m = 30$. Green curves correspond to the parallel direction and blue curves to the transverse direction. Displacements in the parallel direction remain ballistic on numerical time-scales and in the transverse direction the 2D-like diffusive behaviour (see Fig. 1) disappears gradually when $t_{\text{nl}} < t < t_z$. It will be seen further that the diffusive behaviour is recovered in all directions on longer time-scales (i.e. $t \gg t_z$). Fig. 4 presents the evolution of $\langle p_i^2 \rangle / p_{\parallel,0}^2$ in time for $p_{\parallel,0}/(m_e c) \in [1, 10^4]$. Comparing to Fig. 2, one observes that $\langle p_{\parallel}^2 \rangle / p_{\parallel,0}^2$ keeps the same behaviour as in 2D and the transverse components begin to rise at later times; longer time simulations are needed to explore its asymptotic behaviour. Interestingly, a different behaviour is observed for particles with momenta satisfying $t_{\text{nl}} > t_{\parallel,c}$: in this 3D OTSI turbulence, electromagnetic fields reverse every half coherence length along the longitudinal direction, due to the periodicity in that direction; therefore, particles with $t_{\text{nl}} > t_{\parallel,c}$ execute oscillations in the transverse direction, with ballistic motion along the longitudinal direction. Such particles are then confined in the transverse plane because their motion is reversed before they have time to experience a decorrelated field in the transverse plane. This is particularly important with respect to acceleration efficiency, since such particles would not return on a short time-scale (in the absence of a mean field, of course). One can check that the condition $t_{\text{nl}} > t_{\parallel,c}$ amounts to $p_{\parallel,0} > \epsilon_s \gamma_m^2 / 2$ for $\mathbf{p}_{\perp,0} = 0$, which is easily satisfied, or in terms of initial transverse velocity, $\mathbf{p}_{\perp,0} / p_{\parallel,0} < 2 / \gamma_m^2$, which is also generically satisfied for the suprathermal particles. This means that OTSI turbulence is inefficient from the point of view of scattering suprathermal particles away from the longitudinal direction.

In order to test our estimates from Section 3.3, a simulation with enhanced integration time was performed in the case where $p_{\parallel,0}/m_e c = 1$. The result is presented in Fig. 5 where different statistical quantities are plotted as a function of time. A slightly smaller value $\gamma_m = 10$ is adopted here to reduce the characteristic t_z time.

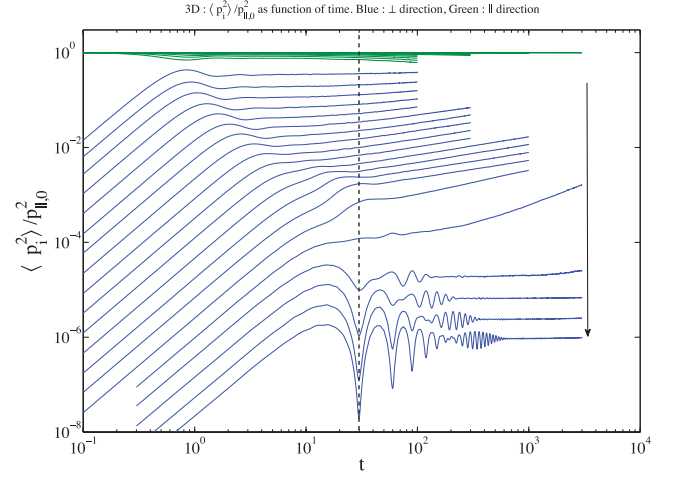


Figure 4. Time evolution of $\langle p_i^2 \rangle / p_{\parallel,0}^2$ for different values of $p_{\parallel,0}/(m_e c)$, in 3D fields. Green curves: parallel (z) direction; blue curves: transverse direction. The dashed vertical line delimits the linear coherence time in z-direction $t_{\parallel,c} = \gamma_m l_{\perp} / c$. Comparing to Fig. 2 $\langle p_{\parallel}^2 \rangle / p_{\parallel,0}^2$ keeps the same behaviour as in 2D and the transverse components begin to rise at later times but longer time simulations are needed to explore its asymptotic behaviour. A different behaviour are observed for particles with momenta satisfying $t_{\text{nl}} > t_{\parallel,c}$, which are confined in a coherence cell in the transverse plane, see the text for details.

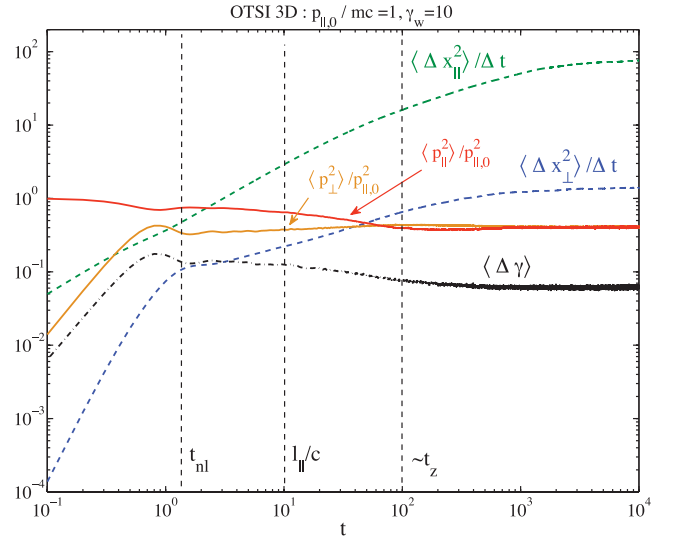


Figure 5. For OTSI modes, time evolution of different quantities in the case $p_{\parallel,0} = m_e c$ with enhanced integration time. The solid curves show the average $\langle p_i^2 \rangle / p_{\parallel,0}^2$, the red colour for parallel direction and the orange colour for the transverse one. The dashed curves show spatial transport coefficients $\langle \Delta x_i^2 \rangle / \Delta t$. Green colour for parallel direction and blue for transverse direction. The dot-dashed black curve shows $\langle \Delta \gamma \rangle$. The vertical dashed lines indicate three characteristic times relevant for particle dynamics. As expected, spatial diffusion is present in all directions on time-scales much longer than t_z . Above the diffusion time all momenta reach isotropy: $\langle p_x^2 \rangle = \langle p_y^2 \rangle = \langle p_z^2 \rangle \simeq p_{\parallel,0}^2 / 3$.

On time-scales larger than t_z the spatial diffusion is recovered in all directions, all momenta are isotropized and energy gain is equal to the field rms energy. Note that the ratio between the spatial transport coefficients in the parallel and transverse directions is not equal to γ_m as expected in equation (33): its value is $55 > \gamma_m$ and scales as $0.6 \gamma_m^2$ when γ_m is varied explicitly in our simulations. It remains

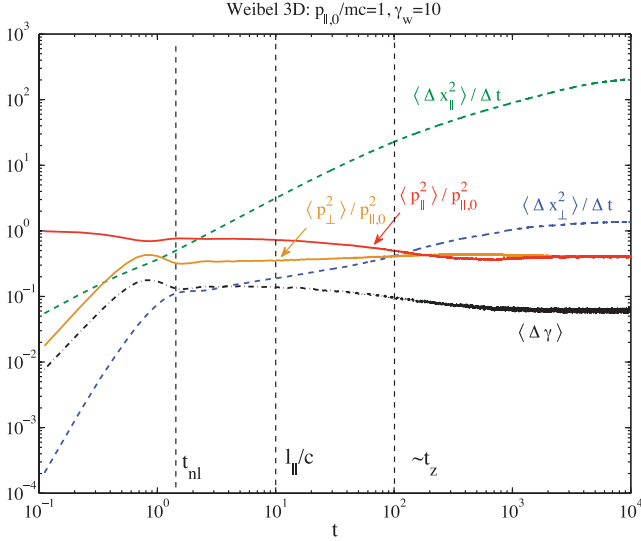


Figure 6. Same as in Fig. 5, but for Weibel 3D modes. Here, we take $k'_{\parallel}/k'_{\perp} = 1/10$. This choice is dictated by numerical time limitation in order to observe the development of a 3D regime. As expected, spatial diffusion is also present in all directions on time-scales much longer than t_z . Above the diffusion time all momentum components reach isotropy: $\langle p_x^2 \rangle = \langle p_y^2 \rangle = \langle p_z^2 \rangle \simeq p_{\parallel,0}^2/3$. We remark that the evolution is very similar to that obtained with OTSI modes, despite the finite range of k'_z wavenumbers.

uncertain if this scaling depends on the choice of low-energy particles [$p_{\parallel,0}/(m_e c) = 1$] and if it remains the same for highest energies. Direct simulations for high energies, with large enough integration time, are numerically prohibitive and are subject to severe numerical errors. In the following, we encode this uncertainty in a parameter χ , which is a substitute for $\ell'_{\parallel}/\ell'_{\perp}$, such that $\chi = \gamma_m$ if the linear value given by equation (33) were to apply, but $\chi \sim \gamma_m^2$ as indicated by the simulations.

Finally, in the Fig. 6, we present also the same simulation but in the case of 3D Weibel-type fields with $k'_{\perp}/k'_{\parallel} = 10$, corresponding to $\kappa = 0.1$. The general behaviour is similar to that observed for transport in OTSI turbulence. In particular, one recovers a scaling $t_z \propto \kappa^{-2}$ and $D_{\parallel}/D_{\perp} \propto \kappa^{-2}$ instead of the linear estimates given in equations (33) and (34), which suggest a scaling in κ^{-1} . As before, we encode this uncertainty with a factor χ , so that $D_{\parallel}/D_{\perp} \simeq \chi$, the simulations indicating $\chi \simeq (\ell'_{\parallel}/\ell'_{\perp})^2$.

As expected, the energy does not undergo a diffusive behaviour. After a limited gain, the particles keep a constant momentum. This is in agreement with theoretical predictions: stochastic acceleration is not seen, transverse heating is bounded, the energetic particle beam is broadened in the transverse direction, but the distribution remains anisotropic.

4 ELECTRON HEATING

As we discussed in Section 2, the wiggler parameter for the background electrons in the proper frame of the microturbulent mode is very large, actually $a \gg \gamma'$, with γ' the typical Lorentz factor of the electrons in that frame. Since the modes carry a transverse electric field that is comparable to the magnetic field, this offers a promising source of preheating in the shock precursor. The growth of the electron temperature together with the growth of electromagnetic waves gives rise to a DC electric field in the normal direction in order to maintain a stationary flow of electrons in the front frame. In turn,

this slows down the incoming proton flow and electron preheating develops at the expense of the kinetic energy of protons.

We first consider the effect of the electric field of the Weibel waves in their proper frame. The electron temperature temporarily increases, as long as their energy is smaller than $e\Delta\Phi' = e\tilde{E}'\ell_{\perp}$, because, in this frame, the total energy of each particle is conserved, as discussed before for suprathermal particles. This limiting energy is

$$\tilde{\epsilon}' = e\tilde{E}'\ell_{\perp} = \xi_B^{1/2}\gamma_m \frac{\ell_{\perp}}{\delta_i} m_p c^2. \quad (36)$$

Reverting to the background plasma frame, that energy corresponds to a temperature which is a sizable fraction of the proton energy:

$$T_{e,\text{lim}} = \xi_B^{1/2}\gamma_m \frac{\ell_{\perp}}{\delta_i} m_p c^2, \quad (37)$$

assuming that most of the electron heating is distributed along the transverse direction. The transverse characteristic size is inflated by the high electron temperature, so that $\ell_{\perp} = \sqrt{\gamma_e}\delta_e \simeq \sqrt{3T_e/m_p c^2}\delta_i$ (see Section 2.1 and Appendix A). Therefore, the temperature in the upstream comoving frame is finally

$$T_{e,\text{lim}|u} = \xi_B m_p c^2, \quad (38)$$

and $\ell_{\perp} \sim \xi_B^{1/2}\delta_i$.

This transitory heating process is not in a diffusion regime, it is rather a direct linear acceleration in the coherent electric field of a coherent cell. Using equation (23), one can easily check that the energy $\tilde{\epsilon}'$ is obtained over a typical linear time-scale ℓ_{\perp}/c . This fast heating in Weibel waves is a particular case of a situation where thermal electrons undergo strong relativistic motions in the waves, reaching relativistic temperatures $T_e \sim a m_e c^2$. A similar process is at work in the OTSI turbulence.

Because the transverse coherence scale is everywhere smaller than the precursor length-scale, on which ξ_B varies, the above-mentioned fast heating process brings forward a picture in which electrons are nearly instantaneously heated to the local temperature given by equation (38), scaling as ξ_B . Of course, as the electrons near equipartition with the ions, one may expect the above heating process to saturate, notably because the oscillation parameter then becomes smaller compared to γ' , as discussed in Section 2. Far from the shock, $\xi_B \ll 1$ hence the electrons are heated to temperatures well below m_p/m_e (upstream frame), while closer to the shock, the temperature rises. Interestingly, PIC simulations indeed show a gradual evolution of the electron temperature over the length-scale of the precursor (Sironi & Spitkovsky 2011a). The above preheating process provides a concrete physical mechanism for this picture.

Note that our analysis differs from the recent proposal of Gedalin et al. (2012), which argues that the background electrons are heated in the inductive longitudinal electric field of the filament. In the present scenario, the electrons oscillate in the transverse electric field in the wave frame, which corresponds through a Lorentz transform to the transverse magnetic field of the filament in the upstream frame.

The above estimate of the electron temperature allows us to evaluate several quantities of interest. The transverse equilibrium of the filament may be described through the relation $\delta n T_e + \delta B^2/8\pi = 0$, assuming that electrons share everywhere the same temperature, with δn the density contrast between the outside and the inside of the filaments. This leads to $\xi_B \approx (|\delta n|/n)T_e/(m_p c^2)$, which, when compared to the above estimate for T_e , suggests $|\delta n|/n \sim 1$. We also note that, using this estimate of the temperature, the filament Lorentz factor becomes of the order of $\gamma_m \sim (\xi_{cr}\xi_B)^{-1/4}$ close to

equipartition and $\xi_{\text{cr}}^{-1/2}$ for $\xi_{\text{B}} \leq \xi_{\text{cr}}$, which should thus increase with the distance to the shock. With $\xi_{\text{B}} \sim \xi_{\text{cr}}$ at the shock front, as suggested in Section 2.3 and as indicated by PIC simulations (Sironi & Spitkovsky 2011a), one finds $\gamma_{\text{m}} \sim \xi_{\text{cr}}^{-1/2}$ close to the shock front.

The electron preheating has an important feedback on the instability: although it does not saturate the instability, it reduces the phase velocity of the Weibel modes, at least because it increases the small mass ratio and determines the condition for the reflection of incoming protons. Regarding OTSI modes, the heating process is similar but it stops with the saturation of the OTSI when the electrons achieve a relativistic temperature.

Across the shock front, the proton heating follows from the mixing of the different proton flows carrying energy of the order of $\Gamma_{\text{s}} m_p c^2$ in the shock front frame. More puzzling is the issue of electron heating. In the previous paragraph, we saw that a significant preheating of the electron is expected. The final stage of electron heating across the shock front is likely related to an effective Joule effect due to scattering. The scattering frequency of thermal particles in the shocked flow is $\nu_{\text{ss}} \sim \xi_{\text{B}} \omega_{\text{pi}}$ and the magnetic diffusivity $\nu_{\text{m}} = \eta c^2 / (4\pi) = \nu_{\text{ss}} \delta_{\text{i}}^2 \sim \xi_{\text{B}} \delta_{\text{i}}^2$. The typical length of Joules dissipation is thus $\ell_{\text{J}} = 3\nu_{\text{m}}/c \sim 3\xi_{\text{B}} \delta_{\text{i}}$, which is a quite short distance for particle thermalization. A more detailed estimate is obtained by looking at the absorption of each Fourier mode, which leads to $\ell_{\text{J}}(\lambda) = 3\lambda^2 / \xi_{\text{B}} \delta_{\text{i}}$. All the magnetic energy that has been generated in the precursor is thus dissipated in the electron heating, and the electron temperature remains in sub-equipartition with that of protons, $T_{\text{e}} \sim \xi_{\text{B}} \Gamma_{\text{s}} m_p c^2$ (shock front frame). It turns out that both processes, preheating and Joules heating, have a similar contribution to the electron temperature that corresponds to the dissipation of the magnetic energy that has been generated by the Weibel instability.

5 APPLICATION TO ACCELERATION AT A GRB EXTERNAL SHOCK

Section 3 provides the tools required to discuss the residence time of particles upstream of a relativistic shock. As discussed in Achterberg et al. (2001) and Pelletier, Lemoine & Marcowith (2009), one must compare the diffusion time-scale in the microturbulence with the time-scale associated with rotation in the background field and keep the shorter of the two. Let us discuss here the implications of the microturbulence. The Weibel filaments are likely the best sites of scattering, since the OTSI modes, at least in their linear description, lead to the confinement of high-energy particles along the shock normal.

The upstream residence time of suprathermal particles returning from the shocked plasma into the upstream flow is that corresponding to a deflection by an angle $1/\Gamma_{\text{s}}$ beyond which the shock front catches up the particle (Gallant & Achterberg 1999; Achterberg et al. 2001); this provides a reasonable estimate of the acceleration time of the Fermi process. This has to be estimated in the filament frame first, in which the required deflection angle is $\sim 1/\Gamma_{\text{fil}}$, with Γ_{fil} the relative Lorentz factor between the shock front and the wave frame, as determined by equation (10). The influence of a possible background magnetic field on the return time-scale is discussed further below. For a particle of energy ϵ_{m} in this wave frame, the residence time is

$$t_{\text{res,m}} \sim \chi \frac{\ell_{\perp}}{c} \left(\frac{\epsilon_{\text{m}}}{\epsilon_{\star}} \right)^2 \frac{1}{\Gamma_{\text{fil}}^2}, \quad (39)$$

where χ is a factor large compared to unity. It accounts for the fact that the decorrelation time in the longitudinal direction is much larger than that in the transverse direction, as discussed above.

For OTSI modes, the simulations indicate $\chi \sim \gamma_{\text{m}}^2$, although the confinement in the transverse plane leads to very ineffective scattering; scattering is rather provided by the Weibel modes, for which $\chi \sim \gamma_{\text{m}}^2 k_{\perp} / k_{\parallel} > \gamma_{\text{m}}^2$, in terms of the wavenumbers of the instability measured in the background plasma rest frame.

Going to the front frame, one finds a residence time-scale:

$$t_{\text{res,f}} \sim \chi \frac{\ell_{\perp}}{c} \left(\frac{\epsilon_{\text{m}}}{\epsilon_{\star}} \right)^2 \frac{1}{\Gamma_{\text{fil}}^3}, \quad (40)$$

with $\epsilon_{\star} = (\gamma_{\text{m}} / \Gamma_{\text{s}}) e \bar{B}_{\text{fil}} \ell_{\perp}$ in terms of the turbulent magnetic field in the front frame \bar{B}_{fil} , and $\epsilon_{\text{fil}} \simeq \Gamma_{\text{fil}} (1 - \beta_{\text{fil}}) \epsilon_{\text{m}}$.

$$t_{\text{res|f}} \sim \chi \frac{\ell_{\perp}}{c} \left(\frac{\epsilon_{\text{fil}}}{e \bar{B}_{\text{fil}} \ell_{\perp}} \right)^2 \frac{\Gamma_{\text{s}}}{\gamma_{\text{m}}}. \quad (41)$$

The fact that the scattering takes place in a frame moving at high speed shortens the residence time, but this gain is mitigated by the anisotropy of the turbulent modes, which induces the χ factor.

5.1 Electron acceleration at relativistic shocks and radiation

We have developed arguments in favour of an efficient heating of the electron fluid by the microturbulence, which confirms the idea that the electrons could likely reach a sub-equipartition temperature at relativistic shocks. For instance, at the external shock of a GRB, where the afterglow radiation is produced, the electrons could achieve a temperature of a few tens of GeV. Indeed, the proton temperature is very high at the beginning of the afterglow, and we have $T_{\text{e}} \lesssim T_{\text{p}} \sim \Gamma_{\text{s}} m_p c^2$, which corresponds to a few tens of GeV. Intense short-scale magnetic turbulence develops because the interstellar magnetization parameter is very low, $\sigma \sim 10^{-9}$.

What kind of radiation can be expected in such a small-scale field, much more intense than the mean field? This depends on the wiggler parameter a , now measured in the downstream frame:

$$a \equiv \frac{e \bar{B}_{\text{c}} \ell_{\text{c}}}{m_e c^2} \sim \xi_{\text{B}}^{1/2} \Gamma_{\text{s}} \frac{m_p}{m_e}. \quad (42)$$

This parameter measures the capability of the magnetic force to deviate a relativistic electron of Lorentz factor γ by an angle $1/\gamma$ (this is the reason for which γ does not appear in the definition). When $a > 1$ the magnetic field produces a single deviation of the electron in the emission cone of half-angle $1/\gamma$, whereas when $a < 1$ the electron can undergo several wiggles in the emission cone. When a is large, the emission behaves like a normal synchrotron radiation in a mean field, except that there is no polarization. When a is small, the emission is of jitter type (Medvedev 2000). In the present case, the large wiggler parameter ensures that the emission caused by shocked and accelerated electrons at a relativistic shock is synchrotron-like; the analysis of the emitted spectrum may provide a diagnosis of the magnetic turbulence although the departures are expected to be moderate (e.g. Fleishman & Urtiev 2010; Kirk & Reville 2010; Medvedev et al. 2011) and actually dominated by the decay dynamics of the microturbulence downstream, which implies that particles of different Lorentz factors cool in regions of different magnetic field strengths (Lemoine 2013).

As for the suprathermal electrons, we find an estimate of the maximum Lorentz factor, measured at shock front, achieved against synchrotron loss; since the acceleration time $\propto \gamma^2 / \bar{B}^2$ and the synchrotron time $\propto \gamma / \bar{B}^2$, the maximum Lorentz factor is independent of the magnetic field intensity. The estimate is similar in spirit to

that derived by Kirk & Reville (2010) up to the dependence on γ_m ; note furthermore that these authors discussed the downstream acceleration time-scale, whereas we include the transport into the upstream. The estimate in the front frame is

$$\gamma_{\max} \sim \left(\frac{4\pi e^2 \ell_c}{\sigma_T m_e c^2} \frac{\gamma_m}{\chi \Gamma_s} \right)^{1/3} \sim (\mu n r_e^3)^{-1/6} \left(\frac{\gamma_m}{\chi \Gamma_s} \right)^{1/3} \\ \sim 7 \times 10^6 \left(\frac{\gamma_m}{\chi \Gamma_s} \right)^{1/3}. \quad (43)$$

To obtain this result, we have taken into account the electron wandering upstream where it experiences a level of turbulence comparable to the downstream one (as measured in the front frame); this level of turbulence is comparable because the extension of the electron trajectory upstream is much shorter than the high-energy proton trajectories that shape the precursor. The corresponding maximum energy of synchrotron photons is

$$\epsilon_{\gamma, \max} \sim \Gamma_s \gamma_{\max}^2 \frac{\hbar e \bar{B}_{lf}}{m_e c^2} \sim \sqrt{\xi_B} \frac{\Gamma_s^{4/3} (\gamma_m/\chi)^{2/3}}{(\mu n r_e^3)^{-1/6}} \frac{m_p c^2}{\alpha_f} \\ \simeq 3 \times \xi_{B,-2}^{1/2} \Gamma_{s,2.5}^2 n_0^{1/2} \left(\frac{\gamma_m}{\chi \Gamma_s} \right)^{2/3} \text{ GeV}, \quad (44)$$

with the usual notation $\xi_{B,-2} = \xi_B/0.01$, $\Gamma_{s,2.5} = \Gamma_s/300$ and $n_0 = n/1 \text{ cm}^{-3}$, and $\alpha_f \simeq 1/137$ the fine structure constant. The maximum photon energy appears stronger than that given by Kirk & Reville (2010), because the level of magnetic energy density in the external shock of a GRB is proportional to the proton mass instead of the electron mass for which only the MeV range would be reached.

The above-mentioned estimate of γ_{\max} balances the acceleration time-scale against the time-scale for synchrotron losses in the turbulent field. In principle, one should also include inverse Compton losses, which puts strict constraints on the return time-scale in the upstream frame, as discussed by Li & Waxman (2006) and Li & Zhao (2011). This requires to use the scattering time-scale discussed above and follow the proper treatment of Klein–Nishina suppression given in these studies; this task is left for future work.

The above discussion considers an unmagnetized shock. In the presence of a background magnetic field, return into the upstream can be achieved through the rotation by an angle $1/\Gamma_s$ in the background field. The return time-scale then corresponds to $t_{\text{res},0f} \sim \epsilon_{lf}/(\Gamma_s e B_0)$ as measured in the shock front frame, so that at the maximal Lorentz factor determined by equation (43):

$$\frac{t_{\text{res},0f}}{t_{\text{res}|f}} \sim 2 \left(\frac{\gamma_m}{\chi} \right)^{2/3} \xi_{B,-2} B_{0,-5}^{-1} n_0^{2/3} \Gamma_{s,2.5}^{1/3}, \quad (45)$$

with $B_{0,-5} = B_0/10 \mu\text{G}$. This implies that the background magnetic field starts to dominate the dynamics of the highest energy electrons as soon as the ratio γ_m/χ becomes significantly smaller than unity, for the above fiducial values. Among others, this guarantees that GeV photons can be produced, independently of γ_m/χ .

Thus, a single synchrotron-like spectrum extending up to several GeV, even possibly a few tens, can be expected and thus is compatible with observations. From that point of view, the efficiency of relativistic shocks with respect to the production of high-energy radiation can be regarded as high.

5.2 Relativistic shock and suprathermal protons in GRBs

As the scattering time increases with ϵ^2 , the Fermi process at relativistic shocks is not expected to be a fast accelerator at the highest energies. For protons, acceleration is in general limited by the dynamical time-scale r_s/c of the shock in the laboratory frame. For the external shock of a GRB at the beginning of the afterglow phase, the maximum energy achieved when the residence time upstream balances the expansion time is

$$E_{\max} = 2Z \Gamma_s \left(\frac{\gamma_m}{\chi} \right)^{1/2} \xi_B^{1/2} \sqrt{\frac{r_s}{\delta_i}} m_p c^2 \\ \sim 3.7 \times 10^{15} \times Z \left(\frac{\gamma_m}{\chi} \right)^{1/2} \Gamma_{s,2.5} r_{s,17} n_0^{1/4} \text{ eV}. \quad (46)$$

Again, the above holds for an unmagnetized shock. As usual, $r_{s,17} \equiv r_s/10^{17} \text{ cm}$. The performance can be improved if one takes into account a background magnetic field, which leads to regular rotation and a shorter return time-scale. The maximum energy can then be written as $E_{\max,0} = Z \Gamma_s e B_0 r_s \simeq 10^{16} \times Z B_{0,-6} r_{s,17} \Gamma_{s,2.5} \text{ eV}$. Thus, although an energy of the order of 10^{16} eV is achieved, the result is far from the range of so-called ultrahigh energy cosmic rays, see also Gallant & Achterberg (1999).

6 CONCLUSIONS AND PROSPECTS

The development of a collisionless shock involves three essential interrelated ingredients: the generation of suprathermal particles, the generation of magnetic turbulence, the building up of a reflecting barrier for a part of the incoming particles. This paradigm applies successfully to non-relativistic as well as to relativistic weakly magnetized shock waves. Numerical and theoretical works have made significant progress in understanding the physics and in providing quantitative results that become useful for astrophysical investigations. This includes not only the spectrum index and cut off of the distribution of accelerated particles, but also the conversion factors into cosmic rays, magnetic turbulence and radiation.

In this paper, we have presented new theoretical investigations regarding the transport of suprathermal particles in the microturbulence upstream of the relativistic shock, and the preheating of the background electrons. We have placed emphasis on the fact that the microturbulent modes actually move relatively the background plasma, with a possibly large Lorentz factor depending on the background electron temperature. This motion of the microturbulence generates a motional electric field in the frame in which the filaments are static, which leads to fast heating of the background electrons through relativistic oscillations. Despite that the Weibel instability generates magnetic filaments – in the background plasma frame – whereas the oblique two stream instability generates almost electrostatic waves, they behave similarly in their proper frame, in which they are composed of an electrostatic field and a magneto-static field of almost the same amplitude. This heating mechanism is particularly efficient: within a transverse coherence length of the perturbations, it heats the electrons to $\sim \xi_B m_p c^2$, in which ξ_B should be understood as the local (position-dependent) fraction of energy density stored in the electromagnetic component. Because the coherence length is much shorter than the size of the precursor, this brings forward the picture in which the electrons are instantaneously heated to the above temperature, so that their temperature rises gradually towards near equipartition as they approach the shock front, a picture which appears in satisfactory agreement with the results

of Sironi & Spitkovsky (2009) and Sironi & Spitkovsky (2011a). As we have discussed, one should expect $\xi_B \sim \xi_{cr}$ at the shock front, from the condition that the Weibel turbulence has become sufficiently strong to reflect the incoming particles. The Weibel turbulence thus apparently draws the maximum amount from the suprathermal particle energy reservoir, in qualitative agreement with PIC simulations.

Electron preheating modifies the generation of microturbulence: it saturates the oblique two stream instability and slows down the propagation of Weibel modes. So, we envisage that the nose of the precursor contains fast propagating Weibel modes and then, closer to the shock front, relativistic thermal electrons that enlarge the characteristic scale. The oblique two stream remain however likely active in the cold phase at the tip of the shock precursor, like Buneman instabilities which also preheat the electrons.

We have also discussed in some detail the properties of transport of the suprathermal particles in the microturbulence. The filamentary nature of the magnetic filaments strongly limits the scattering of these particles in the longitudinal direction. The acceleration process is accordingly slowed down by the time it takes for the particle to probe effectively the inhomogeneities in the longitudinal direction, as quantified here by the factor χ . This strongly suggests that PIC simulations of the Fermi process in 2D probably involves mirror effects on the shock front rather than actual upstream/downstream scattering, especially at the ‘low’ energies corresponding to the first Fermi cycles probed by these simulations. To probe the 3D scattering regime discussed here, one would need 3D PIC simulations with very long integration time-scales, in order to accelerate particles to energies such that their Larmor radius in the turbulent field becomes larger than the coherence length.

Shocks in AGN, blazar jets, or in the internal flow of GRBs are mildly relativistic and therefore not subject to the severe restriction imposed to the Fermi process by the mean field as it happens in the ultrarelativistic regime. Thus, as argued here and in, e.g., Lemoine & Waxman (2009) and Pelletier & Lemoine (2011), those objects are better candidates as sources of ultrahigh energy cosmic rays. In pulsar wind nebulae, reconnections likely contribute to injecting high-energy particles in the shock, and a suprathermal tail with a hard component may be generated (Lyubarsky 2003; Pétri & Lyubarsky 2007; Sironi & Spitkovsky 2011b). At the weakly magnetized external shock of a GRB, Fermi acceleration should be operative and then lead to extended synchrotron spectrum up to GeV energies; although, if the shock propagates in a sufficiently magnetized circumburst environment, the Fermi process may be, in a first step, quenched by the mean field, which would lead to distinct signatures (Lemoine & Pelletier 2011b).

ACKNOWLEDGMENTS

It is a pleasure to acknowledge fruitful discussions with Lorenzo Sironi and Brian Reville, supported by ISSI. This work has been financially supported by the GdR PCHE and the GDRE ‘Exploring the Dawn of the Universe with Gamma-Ray Bursts’ and by the PEPS-PTI Programme of the INP/CNRS.

REFERENCES

- Achterberg A., Wiersma J., 2007, *A&A*, 475, 1
Achterberg A., Gallant Y., Kirk J. G., Guthmann A. W., 2001, *MNRAS*, 328, 393
Achterberg A., Wiersma J., Norman C., 2007, *A&A*, 475, 19

- Bret A., 2009, *ApJ*, 699, 990
Bret A., Firpo M.-C., Deutsch C., 2004, *Phys. Rev. E*, 70, 046401
Chang P., Spitkovsky A., Arons J., 2008, *ApJ*, 674, 378
Fainberg Y. B., Shapiro V. D., Shevchenko V. I., 1970, *Sov. Phys. - JETP*, 30, 528
Fleishman G. D., Urtiev F. A., 2010, *MNRAS*, 406, 644
Gallant Y. A., Achterberg A., 1999, *MNRAS*, 305, L6
Gedalin M., Smolik E., Spitkovsky A., Balikhin M., 2012, *Europhys. Lett.*, 97, 35002
Jones F. C., Jokipii J. R., Baring M. C., 1998, *ApJ*, 509, 238
Keshet U., Katz B., Spitkovsky A., Waxman E., 2009, *ApJ*, 693, L127
Kirk J., Reville B., 2010, *ApJ*, 710, 16
Lemoine M., 2013, *MNRAS*, 428, 845
Lemoine M., Waxman E., 2009, *J. Cosmol. Astropart. Phys.*, 11, 9
Lemoine M., Pelletier G., 2010, *MNRAS*, 402, 321
Lemoine M., Pelletier G., 2011a, *MNRAS*, 417, 1148
Lemoine M., Pelletier G., 2011b, *MNRAS*, 418, L64
Lemoine M., Pelletier G., Revenu B., 2006, *ApJ*, 645, L129
Li Z., Waxman E., 2006, *ApJ*, 651, L328
Li Z., Zhao X.-H., 2011, *J. Cosmol. Astropart. Phys.*, 05, 008
Lyubarsky Y., 2003, *MNRAS*, 345, 153
Lyubarsky Y., Eichler D., 2006, *ApJ*, 647, L1250
Martins S. F., Fonseca R. A., Silva L. O., Mori W. B., 2009, *ApJ*, 695, L189
Medvedev M. V., 2000, *ApJ*, 540, 704
Medvedev M. V., Loeb A., 1999, *ApJ*, 526, 697
Medvedev M. V., Trier Frederiksen J., Haugboelle T., Nordlund A., 2011, *ApJ*, 737, 55
Niemec J., Ostrowski M., Pohl M., 2006, *ApJ*, 650, 1020
Pelletier G., Lemoine M., 2011, in Alecian G., Belkacem K., Samadi R., Valls-Gabaud D., eds, *SF2A-2011: Proc. Ann. Meeting French Soc. Astron. Astrophys.*, p. 39
Pelletier G., Lemoine M., Marcowith A., 2009, *MNRAS*, 393, 587
Pétri J., Lyubarsky Y., 2007, *A&A*, 473, 683
Petrov I., Pelletier G., Lemoine M., 2011, *A&A*, 532, 68
Press W. H., Flannery B. P., Teukolsky S. A., Vetterling W. T., 1986, *Numerical Recipes*. Cambridge Univ. Press, Cambridge
Rabinak I., Katz B., Waxman E., 2011, *ApJ*, 736, 157
Shaisultanov R., Lyubarsky Y., Eichler D., 2012, *ApJ*, 744, 182
Sironi L., Spitkovsky A., 2009, *ApJ*, 698, 1523
Sironi L., Spitkovsky A., 2011a, *ApJ*, 726, 75
Sironi L., Spitkovsky A., 2011b, *ApJ*, 741, 39
Spitkovsky A., 2008a, *ApJ*, 673, L39
Spitkovsky A., 2008b, *ApJ*, 682, L5
Wiersma J., Achterberg A., 2004, *A&A*, 428, 365

APPENDIX A: WEIBEL INSTABILITY WITH A NON-VANISHING PARALLEL WAVENUMBER

Despite detailed analyses of the relativistic beam instability in the Weibel regime, e.g., Wiersma & Achterberg (2004), Achterberg & Wiersma (2007), Achterberg et al. (2007), Shaisultanov et al. (2012) and Bret et al. (2005), the motion of filaments has not been given attention so far. We will emphasize this issue for a cold and a relativistically hot electron fluid.

For a cold background plasma pervaded by a cold monokinetic beam, the wave system is described by the matrix:

$$\Lambda_{ij} = \left(1 - \frac{\omega_p^2}{\omega^2}\right) - \frac{k^2 c^2}{\omega^2} \left(\delta_{ij} - \frac{k_i k_j}{k^2}\right) + \chi_{ij}^b, \quad (A1)$$

where χ_{ij}^b are the components of the susceptibility tensor of the beam plasma given by

$$\chi_{ij}^b = -\xi_{cr} \mu \frac{\omega_{pe}^2}{\omega^2} \left(\delta_{ij} + \frac{k_i v_j + k_j v_i}{\omega - \mathbf{k} \cdot \mathbf{v}_b} + \frac{k^2 c^2 - \omega^2}{(\omega - \mathbf{k} \cdot \mathbf{v}_b)^2} \frac{v_i v_j}{c^2} \right). \quad (A2)$$

We chose a beam velocity direction along z , $\mathbf{v}_b = v_b \mathbf{e}_z$ and a wavevector $\mathbf{k} = k_x \mathbf{e}_x + k_z \mathbf{e}_z$. Electromagnetic waves polarized in the y -direction are decoupled. The wave system of interest reduces to second order, such that

$$\begin{aligned}\Lambda_{xx} &= 1 - \frac{\omega_{pe}^2}{\omega^2} (1 + k_z^2 \delta_e^2 + \xi_{cr} \mu) \\ \Lambda_{xz} &= \Lambda_{zx} = \frac{k_x k_z c^2}{\omega^2} - \xi_{cr} \mu \frac{\omega_{pe}^2}{\omega^2} \frac{k_x v_b}{\omega - k_z v_b} \\ \Lambda_{zz} &= 1 - \frac{\omega_{pe}^2}{\omega^2} (1 + k_x^2 \delta_e^2 + \xi_{cr} \mu) \\ &\quad - \xi_{cr} \mu \frac{\omega_{pe}^2}{\omega^2} \left(\frac{2k_z v_b}{\omega - k_z v_b} + \frac{k^2 c^2 - \omega^2}{(\omega - k_z v_b)^2} \beta_b^2 \right). \quad (\text{A3})\end{aligned}$$

The dispersion relation reads

$$\mathcal{D}(k, \omega) = \Lambda_{xx} \Lambda_{zz} - \Lambda_{xz}^2 = 0. \quad (\text{A4})$$

In the case of Weibel instability, $\omega^2 \ll \omega_{pe}^2$, $k_x^2 \delta_e^2 \sim 1$ and $k_z^2 \delta_e^2 \ll 1$, we find

$$\omega = k_z v_b \left(1 - \xi_{cr} \mu \frac{\gamma_b^{-2} + k_\perp^2 \delta_e^2}{1 + k_\perp^2 \delta_e^2} \right) + i \sqrt{\xi_{cr} \mu} \frac{k_\perp v_b}{(1 + k_\perp^2 \delta_e^2)^{1/2}}, \quad (\text{A5})$$

with $k_\perp = k_x$. This is the result for a cold background plasma and a cold beam. When one takes into account a dispersion of the beam within an angle $1/\Gamma_s$, as previously investigated (Lemoine & Pelletier 2011a; Rabinak et al. 2011), the instability is quenched when $\Gamma_s < (\xi_{cr} \mu)^{-1/2}$. However, the instability is restored when the background electrons are sufficiently hot with both the same growth rate and the same frequency. In the case of OTSI, electron heating up to relativistic temperature tends to quench the instability because the modes become superluminal and thus the resonant interaction cannot be achieved; this effect is however delayed by the fact that the frequency is negatively shifted by the beam, which lowers the phase velocity.

Let us now study a problem similar to the above, albeit for a relativistic electron temperature. As the electrons can come close to equipartition, it is essential to account for the response of the background ions. We thus write the components of the wave tensor:

$$\begin{aligned}\Lambda_{xx} &= \varepsilon_\parallel \frac{k_x^2}{k^2} + (\varepsilon_\perp - \eta^2) \frac{k_z^2}{k^2} + \chi_{xx}^b \\ \Lambda_{xz} &= \Lambda_{zx} = (\varepsilon_\parallel - \varepsilon_\perp + \eta^2) \frac{k_x k_z}{k^2} + \chi_{xz}^b \\ \Lambda_{zz} &= \varepsilon_\parallel \frac{k_z^2}{k^2} + (\varepsilon_\perp - \eta^2) \frac{k_x^2}{k^2} + \chi_{zz}^b, \quad (\text{A6})\end{aligned}$$

where the dielectric coefficients for relativistically hot electrons and cold protons in the low-frequency approximation are

$$\varepsilon_\parallel \simeq 1 - \frac{\omega_{pi}^2}{\omega^2} + \frac{1}{k^2 \lambda_{De}^2} \left(1 + i \frac{\pi}{2} \frac{\omega}{kc} \right) \quad (\text{A7})$$

$$\varepsilon_\perp \simeq 1 - \frac{\omega_{pi}^2}{\omega^2} - \frac{1}{k^2 \lambda_{De}^2} \left(1 - i \frac{\pi}{4} \frac{kc}{\omega} \right). \quad (\text{A8})$$

When considering relativistically hot electrons, it is convenient to write the Debye length λ_{De} such that

$$\lambda_{De}^2 \equiv \frac{T_e}{4\pi n e^2} = \bar{\mu} \delta_i^2 \text{ with } \bar{\mu} \equiv \frac{1}{3} \bar{\gamma}_e \mu \text{ and } \bar{\gamma}_e \equiv 1 + 3T_e/m_e c^2.$$

Whereas the Landau contribution (imaginary part) is a small correction to the longitudinal response, it is dominant in the transverse response.

$$\begin{aligned}\omega^2 \Lambda_{xx} &= \omega^2 \left(1 + \frac{\omega_{pi}^2}{\bar{\mu} k^2 c^2} \right) - \omega_{pi}^2 (1 + \xi_{cr}) \\ \omega^2 \Lambda_{zx} &= \frac{\omega^2}{k^2 \lambda_{De}^2} \left(2 - i \frac{\pi}{4} \frac{kc}{\omega} \right) \frac{k_x k_z}{k^2} + k_x k_z c^2 - \xi_{cr} \omega_{pi}^2 \frac{k_x v_b}{\omega - k_z v_b} \\ \omega^2 \Lambda_{zz} &= \omega^2 \left(1 - \frac{\omega_{pi}^2}{\bar{\mu} k^2 c^2} \right) + i \frac{\pi}{4} \frac{\omega_{pi}^2}{\bar{\mu}} \frac{\omega}{kc} \\ &\quad - \omega_{pi}^2 \left(1 + k_x^2 \delta_i^2 + \xi_{cr} + \xi_{cr} \frac{2k_z v_b}{\omega - k_z v_b} + \xi_{cr} \frac{k^2 c^2 - \omega^2}{(\omega - k_z v_b)^2} \beta_b^2 \right), \quad (\text{A9})\end{aligned}$$

with $\Lambda_{xz} = \Lambda_{zx}$. An important observation is that $\omega_{pb} < \omega_{pi}$, so that one can neglect $|\omega|^2$ in front of ω_{pi}^2 . Furthermore, at equipartition, the ions contribute strongly to the instability and the typical wavenumber $k_x \sim \omega_{pi}$, whereas for $\bar{\mu} \ll 1$, the response of the electrons dominate, and $k_x \rightarrow \bar{\mu}^{-1/2} \omega_{pi}$, the latter corresponding to the relativistic electron plasma frequency. Thus, the dispersion relation can be written (omitting also a term in ξ_{cr}^2 , and assuming $k_z^2 \delta_i^2 \ll 1$) as:

$$\begin{aligned}\left(1 - \frac{\omega^2}{\bar{\mu} k^2 c^2} \right) \left[-i \frac{\pi}{4} \frac{\omega}{\bar{\mu} kc} + 1 + k^2 \delta_i^2 + \xi_{cr} \left(\frac{k^2 c^2}{\delta \omega^2} + \frac{2}{\gamma_b^2} \frac{k_z v_b}{\delta \omega} \right) \right] \\ + 2\xi_{cr} \frac{k_z v_b}{\delta \omega} \left(k_x^2 \delta_i^2 - i \frac{\pi}{4} \frac{\omega}{\bar{\mu} kc} \frac{k_x^2}{k^2} \right) = 0. \quad (\text{A10})\end{aligned}$$

We solve that equation by setting $\delta \omega = \nu + i\gamma$ with the approximation $|\nu| \ll |\gamma|$ (γ should not be confused with Lorentz factors appearing elsewhere). The growth rate is the positive root of the equation:

$$\frac{\pi}{4} \frac{\gamma^3}{\bar{\mu} k^3 c^3} + (1 + k^2 \delta_i^2) \frac{\gamma^2}{k^2 c^2} - \xi_{cr} = 0, \quad (\text{A11})$$

which gives

$$\gamma \simeq \sqrt{\xi_{cr}} v_b \omega_{pi} \frac{k_x \delta_i}{[1 + (k_x \delta_i)^2]^{1/2}}, \quad (\text{A12})$$

provided $(k_x \delta_i)^3 \gtrsim \sqrt{\xi_{cr}}/\bar{\mu}$. If $\bar{\mu} > \sqrt{\xi_{cr}}$, the latter inequality is verified for $k_x \delta_i \gtrsim 1$, which means that the filamentation instability is of the ion-ion type, with typical wavenumber $k_x \sim \delta_i^{-1}$. This represents the range of wavenumbers for which the growth rate peaks, because if $(k_x \delta_i)^3 < \sqrt{\xi_{cr}}/\bar{\mu}$, the Landau effect on hot electrons reduces the growth rate to $\gamma \simeq (4/\pi \bar{\mu} \xi_b)^{1/3} kc$. Now, if $\bar{\mu} < \sqrt{\xi_{cr}}$, the instability is pushed towards higher values of k_x , as the response of the hot electrons dominates.

The frequency shift is obtained at the first order of the expansion in ν :

$$\nu \simeq -k_z v_b \frac{\frac{\pi}{8} \gamma + (k_x \delta_i)^3 \bar{\mu} \xi_{cr} \omega_{pi}}{\frac{3\pi}{8} \gamma + (k_x \delta_i) [1 + (k_x \delta_i)^2] \bar{\mu} \omega_{pi}}. \quad (\text{A13})$$

Using the value of γ and simplifying $1 + (k_x \delta_i)^2 \sim (k_x \delta_i)^2$, one obtains

$$\nu \simeq -k_z v_b \sqrt{\xi_{cr}} \frac{\frac{\pi}{8} + (k_x \delta_i)^3 \bar{\mu} \sqrt{\xi_{cr}}}{\frac{3\pi}{8} \sqrt{\xi_{cr}} + (k_x \delta_i)^3 \bar{\mu}}, \quad (\text{A14})$$

which takes different scalings, depending on the comparison between $\bar{\mu}$ and ξ_{cr} .

If $\bar{\mu} > \sqrt{\xi_{\text{cr}}}$, the filamentation instability grows at $k_x \delta_i \sim 1$, so that

$$\nu \simeq -k_z v_b \frac{\pi}{8} \frac{\sqrt{\xi_{\text{cr}}}}{\bar{\mu}} \quad \left(\bar{\mu} > \sqrt{\xi_{\text{cr}}}, \quad k_x \delta_i \sim 1 \right). \quad (\text{A15})$$

If $\bar{\mu} < \sqrt{\xi_{\text{cr}}}$, maximum growth takes place at $k_x \delta_i \simeq \bar{\mu}^{-1/2}$, so that

$$\nu \simeq -k_z v_b \left(\frac{\pi}{8} \sqrt{\bar{\mu} \xi_{\text{cr}}} + \xi_{\text{cr}} \right) \quad \left(\bar{\mu} < \sqrt{\xi_{\text{cr}}}, \quad k_x \delta_i \sim \bar{\mu}^{-1/2} \right), \quad (\text{A16})$$

although it should be noted that the growth rate increases weakly with $k_x \delta_i$, and that the frequency shift evolves in a non-trivial way with k_x in the interval $\xi_{\text{cr}}^{1/6} \bar{\mu}^{-1/3} \omega_{\text{pi}} \rightarrow \bar{\mu}^{-1/2} \omega_{\text{pi}}$.

We expect that the size of the Weibel filaments, i.e. the transverse coherence length is determined by the maximum k_x ; thus, $\ell_{\perp} \sim \delta_i \sqrt{\bar{\mu}}$ far from equipartition, with $\ell_{\perp} \rightarrow \delta_i$ close to equipartition. For this typical size, the filament Lorentz factor goes from $\gamma_{\text{m}} \sim \xi_{\text{cr}}^{-1/2}$ when $\bar{\mu} < \xi_{\text{cr}}$ to $\gamma_{\text{m}} \sim (\bar{\mu} \xi_{\text{cr}})^{-1/4}$ when $\xi_{\text{cr}} \lesssim \bar{\mu} \lesssim \sqrt{\xi_{\text{cr}}}$, and to $\gamma_{\text{m}} \sim \xi_{\text{cr}}^{-1/4} \bar{\mu}^{1/2}$ for $\bar{\mu} > \sqrt{\xi_{\text{cr}}}$.

The wavelength in the normal direction is limited by $k_z v_b < \gamma$ which implies $\ell_{\parallel} > \delta_i / \sqrt{\xi_{\text{cr}}}$, which is comparable with the growth length.

This paper has been typeset from a \LaTeX file prepared by the author.